Advances in seismic imaging through basalts: a case study from the Faroe–Shetland Basin

Roman Spitzer[1], Robert S. White[1] and iSIMM Team[2]

[1] *Bullard Laboratories, Cambridge University, Madingley Road, Cambridge CB3 0EZ, UK (e-mail: rwhite@esc.cam.ac. uk)*

[2] *See acknowledgements for list*

ABSTRACT: New seismic reflection data have been used to image intra- and sub-basalt features beneath the Faroe–Shetland Basin in the North Atlantic, where the highly reflective top and base boundaries of flood basalts and their complex internal structure make successful seismic imaging difficult. This study demonstrates that appropriate acquisition and processing of marine seismic data from hydrophone streamers and ocean-bottom seismometers (OBS) has the potential to enhance significantly imaging of intra-basalt and sub-basalt seismic reflections. The intersection of a new seismic reflection profile recorded in 2002 with a seismic profile recorded in 1998 allows a direct comparison of advances in sub-basalt imaging over this period and an interpretation of geological structures and seismic velocities at the intersection.

To achieve better resolution of sediments below basaltic layers, surface seismic reflection data using a broad-band, low-frequency source have been recorded. By using a source wavelet with a significantly enhanced frequency spectrum centred at 10 Hz, generated from a large (167 l) airgun array tuned to the first bubble pulse, a wavelet is produced that is capable of penetrating through thick basaltic sequences. Furthermore, recording the low-frequency reflections to large offsets along a 12 000 m long streamer with 3.125 m single sensor spacing allowed effective suppression of multiple reflections, enhanced the precision of velocity analyses and produced better migration results. Seismic data along the same profile were also recorded on a dense deployment of 85 four-component OBS at 2 km or 6 km station spacing. These complementary ocean-bottom data allowed the large-scale velocity variations within and beneath the basalt to be constrained by recording at large offsets the termination of the diving rays (*c.* 18 km) propagating through the basalt.

Integration of seismic reflection data and OBS recordings yields good seismic velocity estimates and, therefore, increased confidence in the interpretation of intra- and sub-basalt features and lithology. Four major stratigraphic units characterized by their seismic velocities and reflection characters were identified: (a) post-basalt sediments; (b) basalt sequence; (c) sub-basalt unit; and (d) the top of presumed Cretaceous basement. The top boundary of the basalt sequence is defined by a strong reflection with a steep velocity increase from 3.5 km s^{-1} to 4.5 km s^{-1} in the *c.* 200 m thick layer above it. The basalt sequence here is *c.* 2.5 km thick. Beneath the base of the basalt there is a velocity decrease from 5.8 km s^{-1} to 5.2 km s^{-1}. The sub-basalt unit is subdivided further into hyaloclastites mixed with sediments and sills, and sub-basalt sediments separated by another velocity inversion from 5.2 km s^{-1} to 4.5 km s^{-1}. The Cretaceous basement with velocities above 5.5 km s^{-1} lies underneath these sub-basalt sediments.

KEYWORDS: *Faroe–Shetland Basin, basalts, seismic imaging, ocean-bottom seismometers*

INTRODUCTION

Imaging prospective structures lying beneath thick basalt flows presents a key challenge in many areas of active hydrocarbon exploration, including the South American and west African continental margins, and many of the sedimentary basins on the northwest European Atlantic margin (Richardson *et al.* 1999). It is difficult to image structures beneath thick basaltic sequences

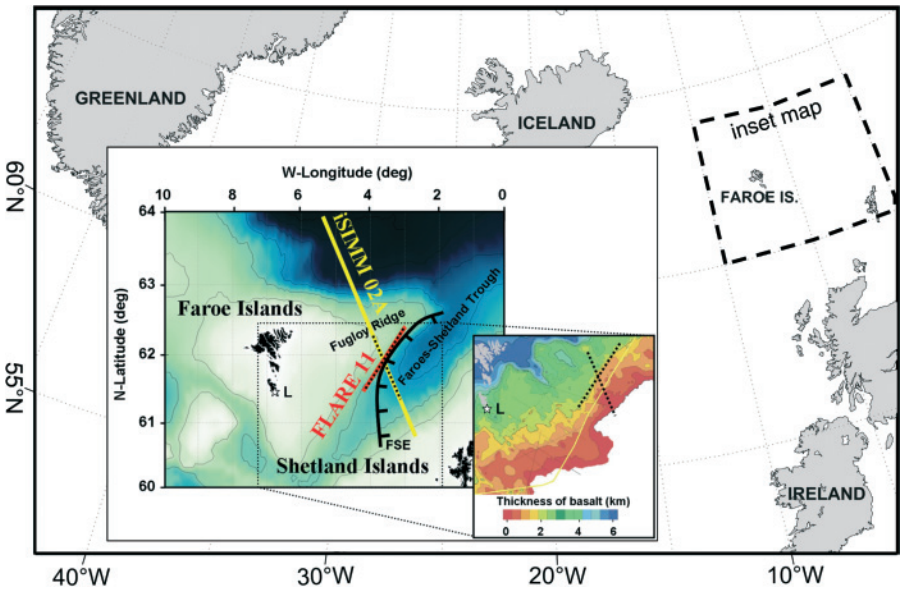

Fig. 1. Map of Faroe–Shetland region (bathymetry contours at 500 m interval) displaying location of iSIMM02A (yellow) and FLARE-11 (red) seismic reflection profiles. Black line indicates Faroes–Shetland Escarpment (FSE). Inset displays thickness of basalt on the Faroes Shelf. Yellow line on inset indicates boundary between UK and Faroese waters. Figure modified from White *et al.* (2003). Black dotted lines along profiles denote portions of seismic reflection data used in this study. L marks location of Lopra borehole. Background map displays North Atlantic region with Faroe Islands highlighted.

using conventional seismic acquisition and processing methods as a consequence of three major effects caused by the layered basalt flows: (i) strong scattering of the seismic wavefield; (ii) high attenuation of transmitted seismic energy; and (iii) multiple generations of peg-leg reflections. Strong scattering is caused mainly by rough boundaries of closely spaced individual basalt flows (Martini & Bean 2002). Further reduction of primary seismic reflection amplitudes occurs as a result of multiple transitions of the wavefront from basalt into intra-basalt sediments or weathered flow tops and *vice versa* (Schönberger & Levin 1974; 1978; Ziolkowski & Fokkema 1986). In general, the complex structure of the internal basalt sequence strongly scatters and highly attenuates seismic energy travelling through it. The sum of these effects causes a relatively low effective Quality factor (Q) of about 35 (intrinsic Q is typically within the range of 100–400) for seismic energy travelling through a typical sequence of stacked basaltic layers (Maresh *et al.* 2003). Further, the generally weak sub-basalt signal may be obscured by peg leg multiple reflections generated at these intra-basalt boundaries.

Detailed investigations of the physical properties of break-up volcanics have led to improved understanding of seismic wave propagation in these volcanic sequences (Planke 1994; Planke & Eldholm 1994) and various approaches have been used to extract information from sub-basalt regions. The application of model-based processing (Hansen *et al.* 2001; Hanssen *et al.* 2003) and inversion techniques (Fruehn *et al.* 1998; 1999; Barton & Barker 2003) are useful for identifying weak sub-basalt features and to support data interpretation. Processing of converted wave energy (Purnell 1992; Barzaghi *et al.* 2002; Van der Baan *et al.* 2003) and sophisticated filter techniques (Spitzer *et al.* 2003) may also enhance the ability to extract additional information about sub-basalt structure contained in seismic reflection data. However, all these techniques are based on recorded data from conventional seismic surveys (i.e. typically 20–100 Hz signals generated and recorded along seismic streamers 3000–6000 m long), which are optimized for high-resolution imaging in horizontally stratified environments dominated by sediments. In an environment dominated by igneous rocks with uneven surfaces and, therefore, a tendency to attenuate the high-frequency components of the seismic wavefield, there will always be difficulties in using these techniques to image the sub-basalt region. Recent investigations have shown that integrated near-offset and wide-angle acquisition (Fliedner & White 2001*a*), combined with a broad-band, low-frequency source (White *et al.* 2002; Lunnon *et al.* 2003), have the potential to overcome some of the aforementioned difficulties when thick layers of igneous rocks are present.

In summer 2002 the iSIMM (*i*ntegrated *S*eismic *I*maging and *M*odelling of *M*argins) consortium successfully completed a seismic acquisition programme on the northwest European Atlantic margin (Fig. 1) with multi-channel seismic (MCS) streamer data and ocean-bottom seismometer (OBS) data acquired along the same line (i.e. iSIMM02A in Fig. 1). This paper highlights the key characteristics of this survey and compares new results with those obtained from the intersecting FLARE-11 seismic reflection profile, which was part of the FLARE programme (*F*aeroes *L*arge *A*perture *R*esearch *E*xperiment) recorded in the late 1990s (Fruehn *et al.* 1998; 1999). It demonstrates further that recording and processing of densely sampled reflection data combined with information contained in long-offset OBS data enhances the ability to obtain velocity estimates from below the basalt, consequently increasing confidence in the interpretation of intra-basalt and sub-basalt features. With the comprehensive iSIMM dataset, accurate seismic velocity estimates constrained by reflection and refraction data were obtained and both the base of the basalt sequence and the top of the underlying Cretaceous basement could be mapped with confidence.

GEOLOGICAL SETTING

The continental margins of the northern North Atlantic are examples of volcanic rifted margins, where a close link between rifting and magmatism can be seen clearly. Along a 2500 km long rift extending from northern Norway to the southern tip of Rockall and along most of the southeastern coast of Greenland, massive intrusive and extrusive magmatism accompanied continental break-up which occurred in the Paleocene. The amount of igneous material extruded at the time of the continental break-up is an estimated $1–2 \times 10^6$ km^3 and the total volume of igneous addition may be as much as $8–10 \times 10^6$ km^3 when intrusives in the lower crust are also considered (White & McKenzie 1989; Eldholm & Grue 1994).

This study focuses on the region near the Faroe Islands (Fig. 1), where the massive outburst of igneous activity at the time of

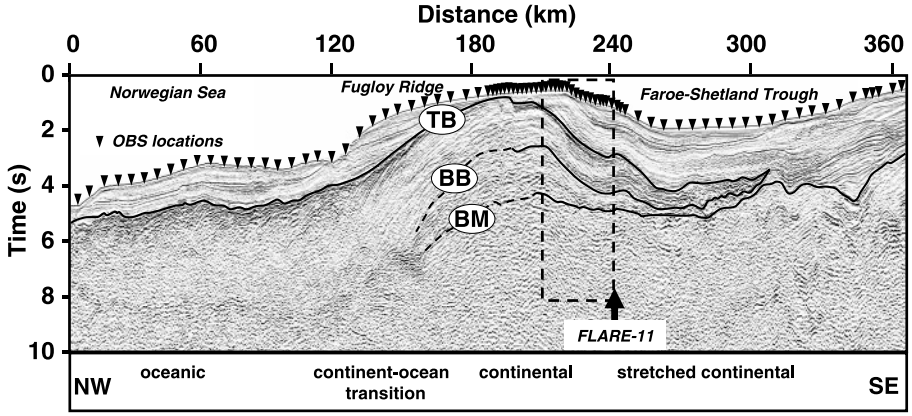

Fig. 2. 375 km long iSIMM02A seismic reflection profiles (see Fig. 1 for location). Black triangles show locations of 85 OBS. Preliminary interpretation of major stratigraphical boundaries is superimposed, TB and BB mark top- and base-basalt horizons, respectively, BM outlines the top of the Cretaceous basement. Dashed box shows region from which data were used in this study; arrow indicates intersection with FLARE-11 profile. iSIMM02A data are shown with permission of WesternGeco.

continental break-up exerts a number of important effects on the surrounding geology of the margins, many of which are particularly relevant to the exploration of hydrocarbons (Doré *et al.* 2002). The addition of large quantities of melt dramatically changed the thermal history in this region, which is of great importance for the maturation of hydrocarbons. Further, knowledge of the volume and distribution of intruded igneous rock in the lower crust is a major factor in estimating the correct subsidence rates in this region, which again affects the maturity of hydrocarbons. Good understanding of such variations is crucial in assessing the hydrocarbon potential of the adjacent basins since they cause rapid regional uplift and subsidence and have been postulated to control sedimentation pulses (White & Lovell 1997). Finally, the lavas flowed *c.* 150 km eastward away from the Atlantic continental margin rift zone which runs north of the Faroe Islands (inset in Fig. 1), feathering out in the Faroe–Shetland Trough (White *et al.* 2003).

Figure 2 shows an overview plot of the entire seismic reflection profile iSIMM02A recorded east of the Faroe Islands, which allows regional geological units across the continent–ocean transition to be mapped. The profile extends from the oceanic crust of the Norwegian Sea in the northwest to the edge of the continental platform in the southeast. It traverses several distinct provinces, including oceanic crust in the northwest, the volcanic continent–ocean transition generated during the Tertiary continental break-up, the Fugloy Ridge in the central part of the profile and the stretched continental crust of the Mesozoic Faroe–Shetland Trough (see annotation along the bottom of Fig. 2).

The major stratigraphic boundaries are marked with bold lines in Figure 2. TB (top basalt) indicates the boundary between flood basalts and overlying post-basaltic sediments and can be followed easily across the entire section. It is the most prominent seismic reflection in the entire dataset. The seismic reflection marked by BB (Fig. 2) from the base of the flood basalts is much more difficult to identify. This horizon is sometimes hard to distinguish from neighbouring seismic events, as beneath the Fugloy Ridge (dashed line in Fig. 2). The identification of the seismic reflection labelled BM from the top-basement (presumed Cretaceous) boundary is also relatively complicated, because of the lower signal-to-noise (SN) ratio of the seismic data beneath the thick sequence of flood basalts. Detailed information on the regional features seen on the iSIMM02A profile in Figure 2 are discussed by White *et al.* (2005).

DATA ACQUISITION

Multi-channel streamer (MCS) data

Table 1 shows the principal acquisition parameters for both the iSIMM02A and FLARE-11 survey. The most significant differences between the two MCS acquisition configurations are the seismic source parameters and the shot and receiver intervals. The number of airguns and their tuning mode, and the total volume of the airgun array, is markedly different between the iSIMM02A and the FLARE-11 profiles. The number of simultaneously active receiver channels (3840 single-sensors spaced 3.125 m apart) used along the iSIMM02A profile was also much greater than along the FLARE-11 profile which was acquired using two ships, each of which recorded 480 receiver groups 12.5 m apart. This resulted in 50 m shot spacing and 12.5 m receiver interval after 'digital group forming' (Ozbek 2000) for iSIMM02A compared with 100 m shot and receiver spacing for the FLARE-11 survey after binning the prestack data. Another advantage of the acquisition system used for the iSIMM02A profile is that shot-by-shot signatures at near-gun hydrophones were recorded to reconstruct the far-field source signature from these individual near-field measurements (Ziolkowski *et al.* 1982).

To compensate for the relatively large amount of seismic energy that is lost in transmission due to the multiple sequence of high-impedance contrasts between individual flows in the basalt section, a large airgun array, comprising 48 airguns with a total volume of 167 l, was used on the iSIMM profile. This large-volume array also compensates for the loss of energy due to scattering and the generation of peg-leg multiple reflections

Table 1. *Principal acquisition parameters of seismic reflection data recorded along iSIMM02A and FLARE-11 profiles, respectively*

	iSIMM02A		FLARE-11
	MCS data	OBS data	MCS data
Geometry			
number of channels	960[a]	4-C	480[b]
shot spacing (m)	50	100	100 flip-flop[b]
receiver spacing	12.5 m[a]	2 and 6 km	100 m[b]
minimum offset (m)	130	0	200
maximum offset (km)	12	375[c]	18
Source			
number of guns per array	48	14	30
volume of gun array, l (in.^{3})	167 (10 170)	104 (6360)	83 (5070)
tow depth (m)	18	20	15
tuning	first bubble	first bubble	first peak
Recording system			
sampling interval (ms)	2	8	4
record length (s)	18	60	18

For details of FLARE-11 profile see Fruehn *et al.* (1998; 1999).
[a]after digital group forming (3840 simultaneously active channels; single sensor spacing is 3.125 m)
[b]after binning into 'supergathers' (single sensor spacing is 12.5 m using two recording passes with two-ship configuration)
[c]useful arrivals up to *c.* 140 km

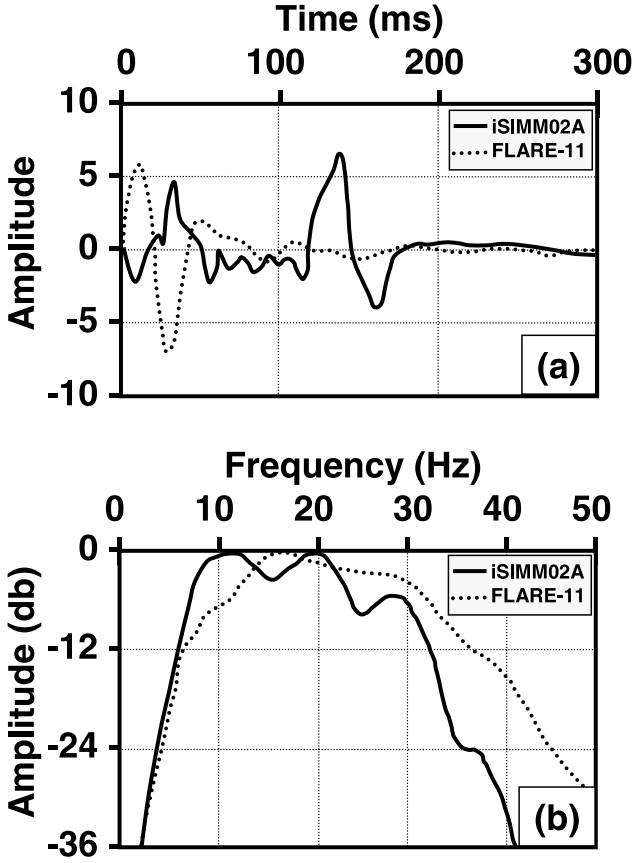

Fig. 3. (**a**) Source signatures used for iSIMM02A (solid line) and FLARE-11 (dotted line) data acquisition. Signatures are scaled with respect to the rms value of the individual signal. (**b**) Frequency spectra for source signatures in (a).

within such a sequence, which cause stacked basalt flows to act as a low-pass filter to seismic waves. Additionally, to increase significantly the amount of low-frequency energy in the seismic signal the airgun array was designed to produce constructive interference of the first bubble pulses of the individual airguns (Avedik *et al.* 1996) rather than conventional tuning on the first peak pulse. The unusually large tow depth of the streamer and airguns of 18 m further enhances the low-frequency, broadband character of the seismic source signature. Details of the seismic source design and characteristics are published by Lunnon *et al.* (2003). Combination of a large-amplitude seismic source and a wavelet which is rich in low frequencies yields an efficient seismic source signature that penetrates through a low-Q medium, such as basalt layers, without unacceptable loss of energy.

Figure 3 shows a comparison of the average source wavelets and their frequency spectra used for data acquisition along the iSIMM02A and the FLARE-11 profiles. The iSIMM02A signature (solid line in Fig. 3a) represents a mixed-phase signal, while the FLARE-11 signature (dotted line in Fig. 3a) is a classical minimum-phase signal with most of its energy in the leading part of the waveform. Both source signatures contain the source ghost and the streamer ghost. Note that the second major peak of the iSIMM02A signature at *c.* 140 ms represents the bubble-tuned peak of the source wavelet, which contains most of the low-frequency energy (Lunnon *et al.* 2003). A consequence of the complicated iSIMM02A signature is that it demands more careful wavelet processing than the FLARE-11 signature, which is a more conventional minimum-phase wavelet. However, using shot-by-shot designature along the

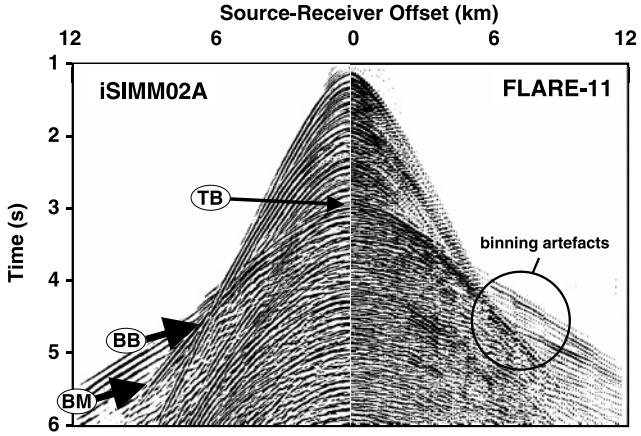

Fig. 4. Raw shot gathers of iSIMM02A (left panel) and FLARE-11 profiles (right panel) recorded at intersection shown in Figure 2. Black arrows indicate TB, BB and BM reflections. Circle highlights binning artefacts in FLARE-11 data. For display purposes geometrical spreading corrections and time-invariant trace balancing have been applied.

iSIMM02A profile allows excellent control to be obtained on the signature in subsequent data processing. Application of a minimum-phasing operator followed by predictive deconvolution and a zero-phasing operator produces a sharp zero-phase wavelet (Christie *et al.* 2004), which allows detailed interpretation of the final migrated sections.

The frequency spectra in Figure 3b underline the differences in the signatures. The diagram shows the frequency content of both signatures between 0 Hz and the respective ghost notches, which are around 40 Hz for the iSIMM02A signature and around 50 Hz for the FLARE-11 spectrum. The difference in the tow depth used in each survey (Table 1) causes the differences in the ghost notch frequency. The FLARE-11 signature yields a slightly broader spectrum at high frequencies because the tow depth was shallower, whereas the iSIMM02A spectrum shows significantly more energy around 10 Hz compared to the FLARE-11 spectrum. The importance of low frequencies in the source wavelet becomes evident after the signal has travelled through the Earth; results from other studies (Ziolkowski *et al.* 2003) illustrate that typically only limited useful information above 20 Hz can be recorded from structure beneath thick basalt sequences.

The use of such a low-frequency source signal combined with a large-aperture streamer allows the recording of high-amplitude, wide-angle seismic reflections from near to and beyond the critical angle of diving waves. This allows one to image interfaces that may be too faint to see on sections derived from near-vertical (short source–receiver offset) seismic reflection data. Acquisition of long-offset data along the iSIMM02A profile, using a single 12 km long streamer allowed large source–receiver offsets to be recorded without any restrictions on source and receiver sampling interval. The long-offset data from the FLARE project used in this paper were acquired using two passes of two ships to reach offsets of up to 18 km along the FLARE-11 profile (Fig. 1). For comparison purposes, in this study a maximum offset of 12 km was selected. Before data processing, the seismic traces recorded by alternate flip-flop firing of the seismic sources on the two ships were re-sorted and binned into 'supergathers' to mimic the data that would have been recorded by a single shot into the synthesized array (for details see White *et al.* 1999).

Figure 4 shows shot gathers recorded at the same location with the sources described above along the iSIMM02A profile

and the FLARE-11 profile. Note that the direction of the profiles is almost perpendicular (Fig. 1), which explains differences on a small scale. However, the subsurface in this area is approximately two-dimensional and, therefore, allows a direct comparison of the major features recorded in these shot gathers. Both shot gathers show the same large-scale features in the subsurface, as reflections from the top (TB) and base (BB) of the basalt sequence. In general, the large number of simultaneously active channels recorded on the iSIMM02A profile (left panel in Fig. 4) produces continuous and unaliased events, which allows more confident identification of single reflected arrivals compared with the conventional shot gather recorded along FLARE-11. The reflected event from the Cretaceous basement (BM) can be seen only on the iSIMM02A data. Further, note that artefacts from re-sorting and binning data into supergathers (such as timing mistakes between individual shot gathers due to streamer feathering) are present in the FLARE-11 shot gather (right panel in Fig. 4), which was recorded using a two-ship configuration.

Ocean-bottom seismometer data

Four-component OBS were also deployed along the iSIMM02A profile (Fig. 2), primarily to facilitate good velocity control and to allow imaging of the deeper crust and the uppermost mantle. This wide-angle OBS profile was acquired separately from the seismic streamer acquisition, using a 104 l (6360 in.^{3}) airgun array towed at 20 m depth (Table 1). The OBS data used in this study were distributed regularly along the line, with a 2 km station spacing (boxed area in Fig. 2). The nominal shot spacing (i.e. trace spacing in OBS record) was 100 m and strong arrivals to maximum offsets of *c.* 140 km were recorded. Traveltime tomography using first arrivals from these recordings is being used to investigate the large-scale velocity structure of the region. Details of the entire OBS dataset and the preliminary results obtained from it are described by Roberts *et al.* (2005).

The first arrival information obtained from wide-angle OBS records can also be used to estimate the thickness of a high-velocity layer, in this particular case the sequence of flood basalt layers. Figure 5 shows the pressure component recorded at the OBS station number 29 (OBS 29), 12 km north of the intersection of iSIMM02A and FLARE-11 profiles. The shots recorded at OBS 29 were fired south of the seismometer, which means that this OBS record samples approximately the same region in the subsurface as the shot gathers shown in Figure 4. For this study, the most significant feature in this OBS record is the termination of the first arrival, which is a diving wave through the basalt, and the step-back to the basement refraction. In this specific OBS example the diving wave terminates at around 18 km source–receiver offset. In addition, note that strong reflected arrivals are recorded between these two major boundaries (i.e. between 5 km and 26 km source–receiver offset). In fact, the step-back of the first arrivals to the basement refraction occurs in two main steps, which indicates the presence of a further major boundary between the base of the basalt sequence and the basement.

Fliedner & White (2001*b*) showed that the diving wave within the basalts will eventually hit the base of the basaltic sequence and encounter a velocity decrease with depth if it is underlain by material with lower velocities, such as sediments – which is the case in the present study. At this point the turning ray terminates and the source–receiver offset at which this termination occurs is, therefore, a measure of the thickness of the basalt. These arrivals appear at large source–receiver offsets, the precise value of which is dependent on the velocity, velocity gradient and thickness of the basalt layer. The diving wave termination is relatively difficult to determine, because the amplitudes of these arrivals decrease gradually beneath the ambient noise rather than terminate abruptly. Therefore, this simple method of estimating the thickness of the basalt layer can yield only an estimate rather than an accurate measurement. Nevertheless, it provides an opportunity to confirm the basalt thickness independently of the velocity estimates derived from conventional reflection data and it can be refined by modelling the amplitudes of the waveforms (Fliedner & White 2001*b*).

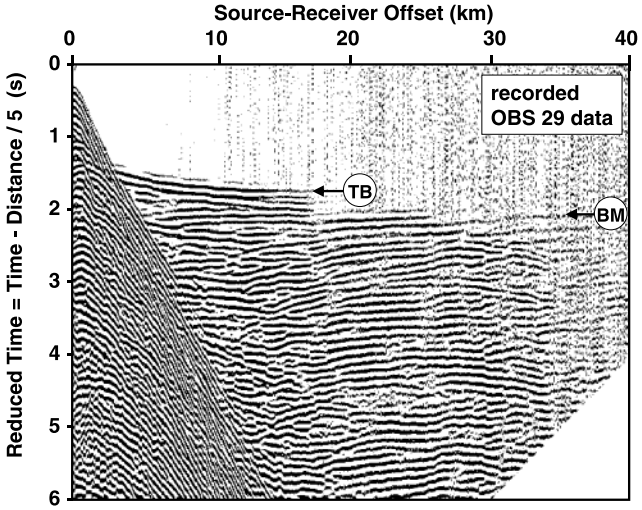

Fig. 5. Hydrophone component of OBS 29 recorded along iSIMM02A profile plotted as reduced travel-time section with 5 km s^{-1} linear moveout velocity. Trace spacing is 100 m (i.e. shot spacing used for the OBS survey). Note the termination of the basalt diving wave (TB) at *c.* 18 km and the step back of the first arrival to the basement arrival (BM). For display purposes automatic gain-control (1 s window length) has been applied.

DATA PROCESSING

The data processing sequences used in this study include a series of robust processing tools (Table 2), which yields a comprehensive sequence designed for the specific needs of sub-basalt imaging. In general, the processing sequences for the iSIMM02A and the FLARE-11 profiles are similar: data pre-processing followed by extensive application of multiple removal techniques, and prestack Kirchhoff time migration has

Table 2. *Processing sequence for seismic reflection data recorded along iSIMM02A and FLARE-11 profiles*

Pre-processing
deconvolution[a]
band-pass filter (0–40 Hz)
F/K filter
geometrical spreading correction
Multiple suppression
surface multiple prediction and subtraction using Kirchhoff integral[b]
removal of events with 1470 m s^{-1} in the parabolic Radon domain
removal of events following picked multiple velocity trend in the parabolic Radon domain[c]
Migration
Kirchhoff prestack time migration
migration velocity analyses (two passes)

[a]iSIMM02A: shot-by-shot designature; FLARE-11: predictive deconvolution.
[b]surface multiple modelling and subtraction using adaptive filter was used for FLARE-11 data.
[c]multiple velocity trend was not picked for FLARE-11 dataset.

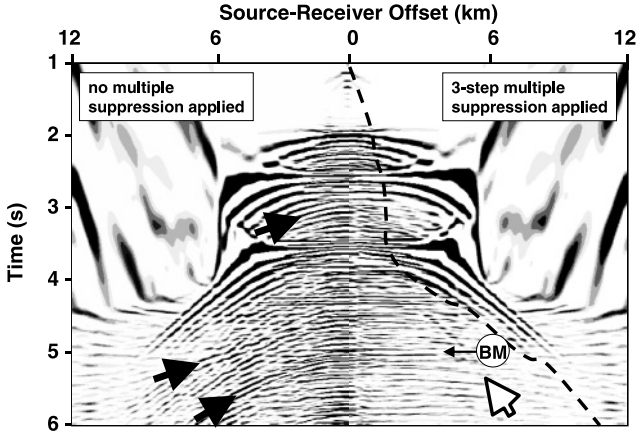

Fig. 6. CMP gather recorded along iSIMM02A profile after scaling, deconvolution and normal moveout (NMO) corrections (left panel). Right panel shows same data after three-step multiple suppression (using sequence in Table 2). Black arrows indicate multiple reflections, white arrow points to converted wave energy and dashed line shows mute function based on 200% NMO-stretch.

been applied to both datasets. Migration velocity analyses provided the detailed interval velocity structures along both profiles and time-to-depth conversions were calculated using these seismic velocities to obtain velocity–depth models for detailed interpretation.

Suppression of multiple reflections

In sub-basalt imaging one of the most important and difficult steps is the elimination of long-period multiples generated between the major impedance boundaries of the free surface, seabed, top-basalt and base-basalt horizons, and the attenuation of peg-leg multiples generated between intra-basalt horizons. The de-multiple strategy for the iSIMM02A profile comprises the prediction and subtraction of multiples using wavefield inversion based on the Kirchhoff integral (Dragoset 1999) followed by the application of two modelling and subtraction passes in the parabolic Radon domain.

Implementation of the surface-related multiple reflection elimination was the preferred approach since the algorithm is not velocity-dependent, and it works effectively even when the sub-basalt velocity profile is uncertain (Hoare *et al.* 2005). In this case it was used solely for removing water-column multiples and worked best in attenuating multiple energy in the near-offset range (i.e. 0–4 km). In addition, modelling and subtraction in the parabolic Radon domain was applied to remove remaining water-column multiples in the mid-offset (i.e. 4–8 km) and long-offset (i.e. 8–12 km) ranges. Finally, in combination with multiple-trend velocity picking, a second pass of modelling and subtraction of multiple reflections generated by the top-basalt horizon was performed. The result of this approach is illustrated in Figure 6. The level of multiple reflected energy is reduced markedly by this processing sequence. A significant result is that after the multiple suppression sequence, the reflection from the basement (marked BM on Fig. 6) is considerably less compromised by strong multiple arrivals at the same two-way-travel time.

Records of the shot-by-shot signatures and continuous spatial sampling along the individual shot gathers are both crucial prerequisites for multiple attenuation using wavefield inversion based on the Kirchhoff integral. Without individual source signature recordings along the iSIMM02A profile and without the dense source and receiver spacing, this comprehensive de-multiple approach would not have been as successful as

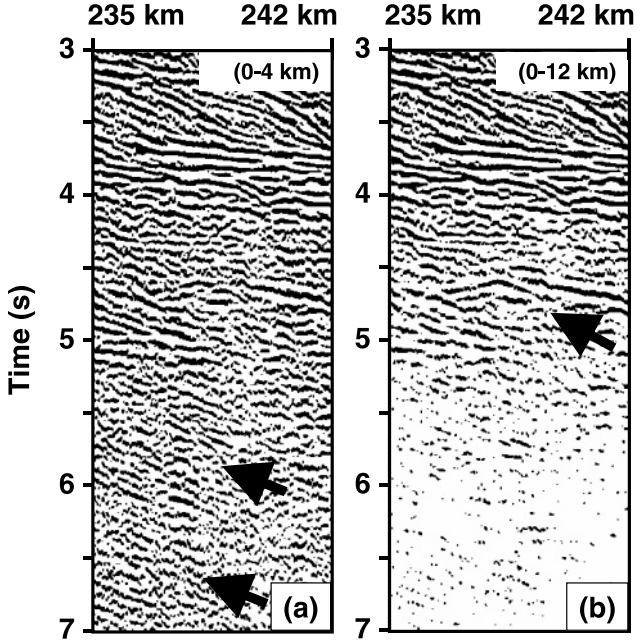

Fig. 7. Stacked data after scaling, deconvolution and multiple suppression extracted from iSIMM02A profile (between distances 232 km and 242 km in Fig. 2), where (**a**) includes only near-offset traces from 0–4 km and (**b**) includes the entire source–receiver offset range from 0–12 km. Arrows in (a) show remnants of stacked multiple reflected energy. Arrow in (b) indicates reflection from basement.

it was. The relatively coarse spatial sampling along the FLARE-11 profile makes the elimination of first-order multiples using wavefield inversion more difficult. Instead a two-step approach (Table 2) was applied, including wavefield prediction and subtraction through modelling, which worked well for the near-offset traces. The relatively lower SN ratio below the top-basalt reflector on the FLARE-11 profile compared to the iSIMM02A profile does not allow a multiple-velocity trend to be picked on the FLARE-11 profile and, therefore, modelling and subtracting multiple arrivals from mid- and far-offsets in the parabolic Radon domain was the preferred choice for reducing the impact of multiples.

Importance of long source–receiver offset data

Since the high-velocity contrast at a sediment–basalt interface causes large ray-bending at non-normal angles of incidence, a significant part of the seismic energy appears at larger source–receiver offsets than in regions without high-velocity layers. This far-offset part of the wavefield also is less influenced by peg-leg multiples, generated at intra-basalt boundaries, which occur mainly in the near-offset range of the recordings. Therefore, to obtain a clear image from sub-basalt regions it is important to record arrivals at large source–receiver offsets.

Figure 7 highlights the effect of using long source–receiver offset-ranges on the final stacked section after scaling, deconvolution and the suppression of multiple reflections. A comparison of near-offset (i.e. 0–4 km) stacked data in Figure 7a with the full-offset range (i.e. 0–12 km) stack in Figure 7b, illustrates that the sub-basalt region (i.e. below *c.* 4 s) is difficult to interpret in Figure 7a relative to the data shown in Figure 7b; too many peg-leg multiple reflections remain in the near-offset range of the data. In comparison, the full-offset section (i.e. 0–12 km) in Figure 7b, which is less influenced by multiple events, shows a much clearer appearance of individual reflections in the sub-basalt area. This comparison shows that a

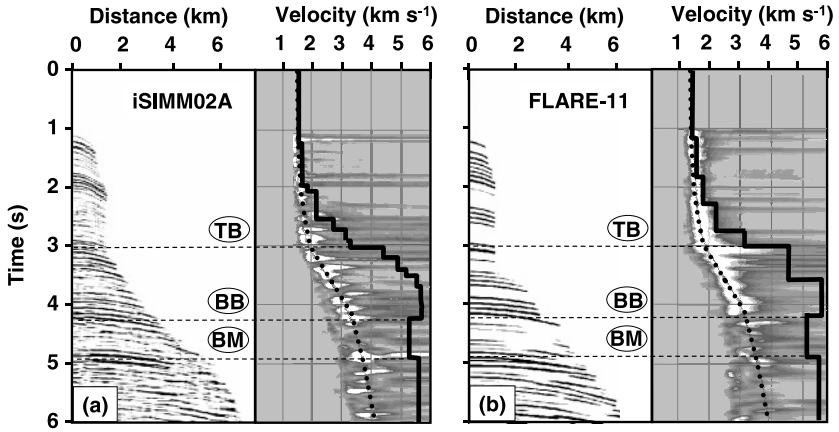

Fig. 8. CMP supergathers (i.e. three adjacent CMP gathers stacked) and semblances recorded along (**a**) iSIMM02A profile and (**b**) FLARE-11 profile. For display purposes automatic gain-control (1 s window length) and time-invariant trace balancing have been applied to the CMP data. Semblance plots show stacking velocity function (dotted line) and interval velocity function (solid line) superimposed.

significant amount of reflected seismic energy is present at source–receiver offsets beyond 4 km. Therefore, it is essential to record seismic traces in the far-offset range to improve the final section (Fig. 7b) by stacking relatively clean (i.e. multiple-free) far-offset data onto near-offset data, which can be contaminated with remaining multiple energy.

Velocity analyses

The accurate estimation of intra-basalt seismic velocities and seismic velocities beneath the basaltic sequence is also essential for successful sub-basalt imaging. Without accurate seismic velocities it is difficult to image detailed features in the complicated region beneath igneous rocks and, furthermore, to characterize sub-basalt lithologies. Figure 8 shows CMP supergathers recorded at the intersection of the iSIMM02A profile and the FLARE-11 profile after Kirchhoff prestack time migration, and the calculated semblance plots at this location.

Within the sediments above the basalt it is straightforward to estimate stacking velocities (dotted lines in Fig. 8), and to calculate the corresponding interval velocities (solid lines in Fig. 8) based on Dix's equation. With the high-quality iSIMM02A data it is also possible to obtain detailed interval velocity estimates within the basalt (between TB and BB, Fig. 8a). A similar gradient within the high-velocity layer generated by the basalt can also be found in the semblance plot derived from the FLARE-11 data (Fig. 8b), but with fewer details than seen on the data from the iSIMM02A profile (Fig. 8a). From both datasets a velocity inversion is found in the deeper part of the data at *c.* 4.2 s. This velocity inversion recorded on both profiles is important, since it indicates the location of a possible interface between the high-velocity basalt sequence and the low-velocity sub-basalt region. From a hydrocarbon exploration perspective this is also an important boundary, because it marks the interface where the top of the prospective structures might lie. However, the observed velocity inversion is relatively small and the results from standard velocity analyses using seismic reflection data alone are insufficient to assign this confidently to a basalt–sediment interface. Another constraint on this velocity inversion is needed and can be found from OBS records that sample the same sub-basalt region (Fig. 5).

When analysing seismic reflection data, observations in OBS records can be used to confirm the velocity estimates derived from conventional velocity analyses. In the present study, the time-to-depth converted version of the interval velocity function described in Figure 8a served as a 1D velocity–depth model for the ray-theoretical travel-time calculation of the termination offset for the diving wave in the OBS record as described by Fliedner & White (2001*b*):

$$x_{\max} = 2\left(\frac{\sqrt{v_{\max}^2 - v_0^2}}{a} + \sum_{i=1}^{n}\frac{z_i v_i}{\sqrt{v_{\max}^2 - v_i^2}}\right) \quad (1)$$

where $x_{\max}$ is the termination offset, a is constant vertical velocity-gradient within the basalt, v_0 is the velocity at the top and $v_{\max}$ at the bottom of the gradient layer, and n is the number of constant-velocity (v_i) overburden layers each with thickness z_i. Substituting into equation (1) a=0.5 (m s^{-1}) m^{-1}, v_0=4500 m s^{-1}, $v_{\max}$=5800 m s^{-1} and n=3 overburden layers estimated from the data shown in Figure 8a, yields a ray-theoretical termination offset of *c.* 18 km, which is consistent with the observed termination of the basalt diving rays in the recorded OBS data in Figure 5.

Comparison of migrated data

Figure 9 shows enlarged areas of the iSIMM02A and the FLARE-11 profiles at their intersection point (Fig. 2), after prestack time migration has been applied. The major features

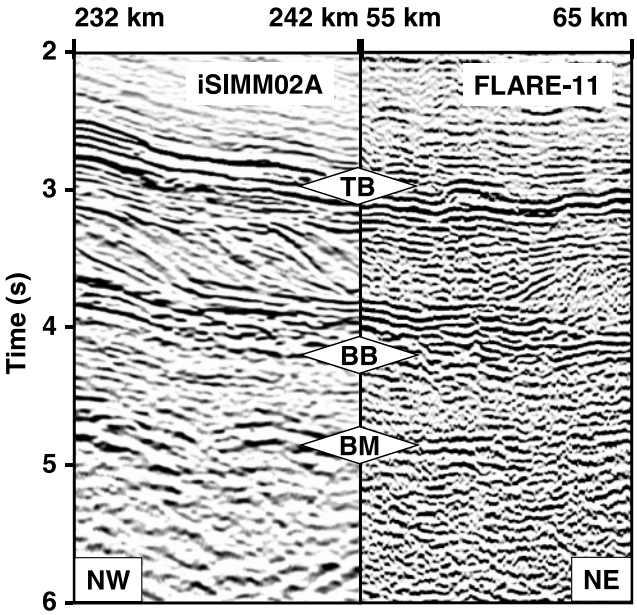

Fig. 9. Enlarged prestack time-migrated sections recorded at intersection of iSIMM02A profile (left panel) and FLARE-11 profile (right panel). Note improved SN ratio in the left panel, especially the high-resolution of intra- and sub-basalt sequence. TB (top-basalt), BB (base-basalt) and BM (Cretaceous basement) lithological boundaries as shown in Figure 2.

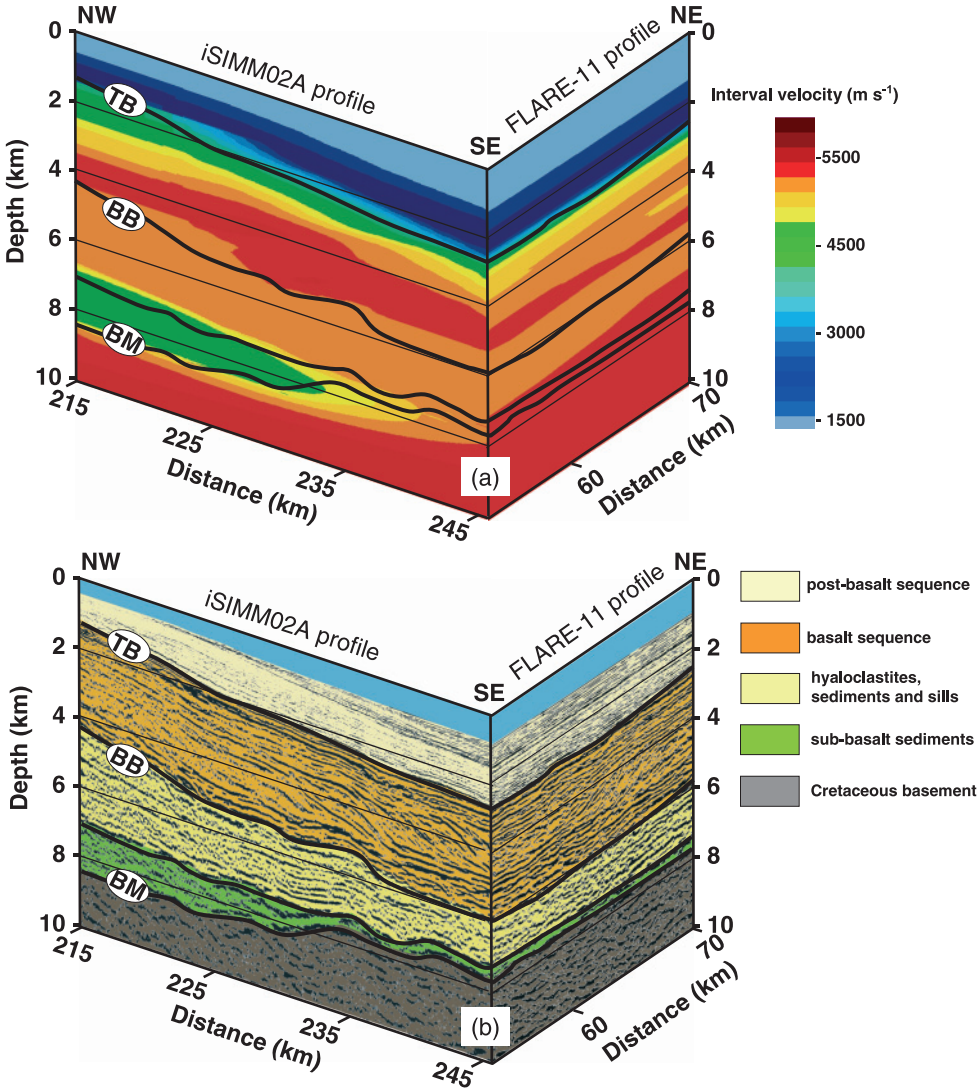

Fig. 10. (**a**) Interval velocity field in depth derived from migration velocity analyses. (**b**) Time-to-depth-converted migrated sections obtained from iSIMM02A and FLARE-11 data, with preliminary interpretation superimposed. For further explanation see text.

can be observed clearly in both profiles. However, it is evident that the SN ratio in the FLARE-11 data decreases more rapidly compared to the SN ratio of the iSIMM02A data. In general, below the top-basalt reflection the low-frequency components of the iSIMM02A data yield more continuity along individual reflections and, therefore, result in a much clearer image compared to the result obtained from FLARE-11 data. Note, especially, the detailed image of the internal structure of the massive basaltic sequence from *c.* 3–4 s. The high data quality allows reflections from major basalt deposits to be identified. Furthermore, features below this sequence can be seen clearly down to *c.* 5 s (i.e. interpreted Cretaceous boundary) and below, whereas these features are hard to identify on the migrated FLARE-11 section alone.

RESULTS

Figure 10 shows a detailed insight into interval velocities and prestack time-migrated data recorded along the iSIMM02A profile and along the FLARE-11 profile (area indicated in Fig. 2). The velocity field in Figure 10a was derived by examining prestack time-migrated image gathers at 1 km spacing. The velocity field along the FLARE-11 profile was obtained by analysing image gathers, starting at the intersection with the iSIMM02A profile to ensure a perfect match of both velocity fields at the intersection point. The seismic velocities along these sections are then linked with the stratigraphic interpretation and the appearance of the various seismic facies in the final migrations (Fig. 10b). The interpretation is consistent with results from previous surveys, which are published by Sørensen (2003).

Velocity–depth structure

The low-frequency content in the seismic source signature and the closer source–receiver spacing along the iSIMM02A profile yields more details and more continuity in the seismic reflections than in the results obtained from the FLARE-11 data (Fig. 9). Therefore, the interval velocity functions derived from data recorded along the iSIMM02A profile are generally more detailed than the seismic velocity profile obtained from the FLARE-11 data. However, both datasets allow a comprehensive velocity analysis to be made, further confirmed by OBS data analyses (Fig. 5), and the interval velocity is therefore used as another attribute to characterize the different seismic facies found in the migrated data.

The velocities within the post-basalt sediments vary between *c.* 1.6 km s^{-1} at the seafloor to *c.* 2.8 km s^{-1} at the top-basalt boundary (Fig. 10a). Below this a steep velocity gradient occurs in the first *c.* 200 m of the basaltic sequence, which is caused by the transition from relatively soft sediments, through more compact ash and tuff deposits to the massive flood basalt flows

which underlie them. The interval velocity within the *c.* 2.5 km thick basalts shows a continuous increase from *c.* 4.5 km s^{-1} at the top to *c.* 5.8 km s^{-1} at the bottom, which might be explained by increased confining pressure resulting in the closure of cracks and the infilling of pore space and cracks by secondary mineralization. At a depth of *c.* 5 km a velocity inversion from *c.* 5.8 km s^{-1} to *c.* 5.2 km s^{-1} occurs in both datasets, indicating the boundary between massive basalt flows and hyaloclastites underneath. Along the iSIMM02A profile another velocity inversion can be observed at a greater depth of *c.* 7 km (Fig. 10a), which may be caused by sub-basalt sediments that pre-date the igneous activity. The relatively low velocity of *c.* 4.5 km s^{-1} of these sub-basalt sediments can be estimated only where the sediments are thickest, namely at around 225 km distance along the iSIMM02A profile. In areas where the sediments are only thin (i.e. *c.* 200 m), as they are on the southern part of iSIMM02A and along the entire FLARE-11 profile (Fig. 10b), this velocity inversion is hidden. The relatively high velocities of the overlying hyaloclastites and the underlying Cretaceous basement mask the velocity inversion caused by the sediments.

Seismic facies and interpretation

The post-volcanic development in the Faroes–Shetland Trough comprises sediments from the Early Eocene up to the present day at the seafloor. This seismic facies is characterized by moderate amplitude, continuous seismic reflections along both profiles (light yellow region in Fig. 10b). The orange-coloured region in Figure 10b (between horizons marked TB and BB) denotes the basaltic sequence, which was extruded during the Late Paleocene. The top boundary of this sequence is the most prominent feature along both profiles. It shows the highest amplitude reflections throughout the entire datasets (other than reflections from the seabed) and is characterized by a change to higher seismic velocities beneath it (Fig. 10a). The basaltic sequence itself shows strong and mainly continuous reflections and a vertical velocity gradient of 0.5 (km s^{-1}) km^{-1} (Figs 8 and 10a).

The seismic facies beneath the basalt flows (yellow region in Fig. 10b, below BB), is also part of the volcanic phase, but is clearly distinct from the flood basalt sequence, as indicated by the velocity inversion from *c.* 5.8 km s^{-1} to *c.* 5.2 km s^{-1} at the BB boundary (Figs 8 and 10a). Furthermore, the reflection character also changes from high amplitudes and strong continuous events within the basalt sequence to relatively low amplitudes and only moderately continuous horizons below the basalts. The relatively high seismic velocity of *c.* 5.2 km s^{-1} is greater than expected for compacted sediments without any igneous component, and suggests that this sequence contains a considerable quantity of basaltic material (i.e. heterogeneous hyaloclastite basalt breccias interbedded with tuffs, sediments and probably also sills).

The interpreted sub-basalt sediments (green regions in Fig. 10b) along the iSIMM02A profile which are marked by the low velocities (green in Fig. 10a) are characterized further by low-frequency and low-amplitude events compared with the neighbouring facies. This seismic facies can hardly be seen on the FLARE-11 data, where it is very thin. The interpretation of this facies along the FLARE-11 section is based on the data recorded along iSIMM02A, which has been extended from the intersection of these profiles in both directions. The seismic velocity of *c.* 4.5 km s^{-1} within this region helps to identify it as consisting of sediments deposited prior to the outburst of volcanism. In contrast, the reflection from the presumed Cretaceous basement (brown regions in Figure 10b, the top of which is marked BM) can be seen clearly on both the iSIMM02A and FLARE-11 profiles. This BM boundary is characterized by relatively high-amplitude reflections and strong continuity in the final migrated section compared to the overlying sub-basalt sediments.

CONCLUSIONS

The ability to image seismically the subsurface below basalts at many locations world-wide is limited by the fact that basaltic layers are characterized by poor seismic penetration caused by high reflectivity contrasts at the top-basalt boundary and at intra-basalt discontinuities, by attenuation and by strong internal scattering of seismic energy. To address these problems, low-frequency, broad-band seismic data employing a 12 000 m long seismic streamer have been recorded across the Faroe–Shetland Trough (Fig. 1). The intersection of the recorded iSIMM02A dataset and the FLARE-11 profile (Fig. 2), which was recorded in 1998, allows a direct comparison to be made between the data quality obtained from an up-to-date, high-end seismic acquisition system with that from acquisition systems typically used in the late 1990s.

An important aspect of the ability to penetrate basalts is the use of low frequencies in the seismic source, as illustrated in Figures 3 and 4. Applying bubble-tuning for the acquisition of the iSIMM02A profile compared to conventional peak-tuning used for the FLARE-11 profiles, combined with a significantly larger total airgun array volume for the former (i.e. 167 l compared with 83 l), yields a seismic source signal that is richer in low frequencies around 10 Hz. As a result of the typical low-pass character of a sequence of basalt flows, relatively more coherent seismic energy from within and beneath the basalts is recorded with the iSIMM02 acquisition strategy.

It is also important to acquire wide-angle data of up to 12 000 m offset in this specific case in order to improve the final seismic image. A comparison of stacks obtained from different source–receiver offset ranges (i.e. 0–4 km and 0–12 km in Fig. 6) reveals that a significant amount of reflected seismic energy is contained in the far-offset traces, which results in a stacked section with much clearer resolution of individual events at depth. In addition to the recording of the iSIMM02A seismic reflection profile, data at 85 four-component OBS with 6 km or 2 km spacing were acquired along the same line. Recordings of basalt diving waves and events generated at the Cretaceous basement in the OBS data contribute significantly to a better understanding of the large-scale geological structures. Furthermore, these data, combined with information from the seismic reflection data at the intersection of the iSIMM02A and FLARE-11 profiles, allow detailed investigations to be made of the seismic velocities in this region (Fig. 5).

Detailed analysis of interval velocities along the seismic reflection lines, combined with independent observations of diving wave termination offsets in individual OBS records, results in accurate velocity fields along both the iSIMM02A and FLARE-11 profiles (Fig. 10a). The accuracy of seismic velocities not only plays an important role in the seismic imaging itself (and particularly in prestack depth migration) but is also vital for the correct interpretation of intra-basalt and sub-basalt structures (Fig. 10b). The combination of reflection character and seismic velocity as the major properties of a seismic facies is a powerful tool for distinguishing different lithologies successfully. Applying this interpretative approach, four major lithologies can be distinguished: (1) post-basalt sediments; (2) basaltic sequence; (3) sub-basalt unit (subdivided further into hyaloclastites and sub-basalt sediments); and (4) presumed Cretaceous basement.

This study demonstrates that recording low frequency, long-offset data significantly improves confidence in the processing, imaging and subsequent interpretation of intra-basalt and sub-basalt features. The seismic reflection data reveal small-scale structures in this highly complex environment and, in combination with the long-offset OBS recordings, provide accurate information on the seismic velocities within and below the basalts, which are important both in interpreting the lithologies and in improving the quality of the seismic imaging.

The iSIMM02A streamer data used in this article were acquired by WesternGeco using their Q-Marine system. WesternGeco also provided the Omega software to process the iSIMM data. The iSIMM (integrated Seismic Imaging and Modelling of Margins) study group comprises R. S. White, N. J. Kusznir, A. M. Roberts, P. A. F. Christie, R. Spitzer, R. Healy, J. Eccles, N. Hurst, Z. C. Lunnon, C. J. Parkin, A. W. Roberts, L. K. Smith and V. Tymms. The authors also wish to thank Anusha Surendra for detailed velocity analyses along the FLARE-11 profile. iSIMM is supported by the UK's Natural Environment Research Council and the Department of Trade and Industry, Amerada Hess Ltd, Anadarko, BP, ConocoPhillips, ENIUK, Shell, Statoil and WesternGeco. The OBS were provided by GeoPro GmbH. The FLARE data used in this article were collected by Amerada Hess Limited and its partners LASMO (ULX) Limited, Norsk Hydro a.s., DOPAS and Atlantic Petroleum. University of Cambridge contribution number ES8089.

REFERENCES

Avedik, F., Hirn, A., Renard, V., Nicolich, R., Oliver, J.L. & Sachpazi, M. 1996. Single bubble marine source offers new perspectives for lithospheric exploration. *Tectonophysics,* **267**, 57–71.

Barton, P. & Barker, N. 2003. Velocity imaging by tau-p transformation of refracted seismic traveltimes. *Geophysical Prospecting,* **51**, 195–203.

Barzaghi, L., Calcagni, D., Passolunghi, M. & Sandroni, S. 2002. Faeroe sub-basalt seismic imaging: a new iterative time processing approach. *First Break,* **20**, 611–617.

Christie, P. A. F., Langridge, A., Lunnon, Z., Roberts, A. W. & the iSIMM team. 2004. iSIMM looks beneath basalt for both industry and university research. Abstract number 87, presented at the 5th Conference and Exposition on Petroleum Geophysics, India.

Doré, A.G., Cartwright, J.A., Stoker, M.S., Turner, J.P. & White, N.J. (eds) 2002. *Exhumation of the North Atlantic Margin: Timing, Mechanisms and Implications for Petroleum Exploration*. Geological Society, London, Special Publications, **196**.

Dragoset, B. 1999. A practical approach to surface multiple attenuation. *The Leading Edge,* **18**, 104–108.

Eldholm, O. & Grue, K. 1994. North Atlantic volcanic margins: dimensions and production rates. *Journal of Geophysical Research,* **99**, 2955–2988.

Fliedner, M.M. & White, R.S. 2001*a*. Sub-basalt imaging in the Faeroe–Shetland Basin with large offset data. *First Break,* **19**, 247–252.

Fliedner, M.M. & White, R.S. 2001*b*. Seismic structure of basalt flows from surface seismic data, borehole measurements, and synthetic seismogram modelling. *Geophysics,* **66**, 1925–1936.

Fruehn, J., White, R.S., Richardson, K.R. *et al.* 1998. FLARE – A two-ship experiment designed for sub-basalt imaging. *68th Annual International Meeting of the Society of Exploration Geophysicists*. SEG, New Orleans, 94–97.

Fruehn, J., White, R.S., Fliedner, M.M. *et al.* 1999. Large-aperture seismic: Imaging beneath high-velocity strata. *World Oil,* **220**, 109–113.

Hansen, J.O., Tjøstheim, B.A. & Sønneland, L. 2001. Analysis of Long Offset Sub-Basalt Data using Model-based Processing. *71st Annual International Meeting of the Society of Exploration Geophysicists*, 1949–1952.

Hanssen, P., Ziolkowski, A. & Li, X. 2003. A quantitative study on the use of converted waves for sub-basalt imaging. *Geophysical Prospecting,* **51**, 183–193.

Hoare, R., Schearer, P., Langridge, A., Saragoussi, E. & Christie, P.A.F. 2005. Imaging sub-basalt with deep towed streamer: a case study from the Faroe Islands. *In:* Ziska, H., Varming, T. & Bloch, D. (eds) Faroe Islands Exploration Conference: Proceedings of the 1st Conference. *Annales Societatis Scientiarum Færoensis,* Supplementum 43, Tórshavn, 168–175.

Lunnon, Z., Christie, P.A.F. & White, R.S. 2003. An evaluation of peak and bubble tuning in subbasalt seismology: modeling and results from OBS data. *First Break,* **21**, 51–56.

Maresh, J., Hobbs, R.W., White, R.S. & Smallwood, J.R. 2003. Attenuation of Atlantic Margin Basalts using downhole VSP. *73rd Annual International Meeting of the Society of Exploration Geophysicists*, 1310–1313.

Martini, F. & Bean, C.J. 2002. Interface scattering versus body scattering in sub-basalt imaging and application of prestack wave equation datuming. *Geophysics,* **67**, 1593–1601.

Ozbek, A. 2000. Adaptive beam forming with generalized linear constraints. *70th Annual International Meeting of the Society of Exploration Geophysicists*, 2081–2084.

Planke, S. 1994. Geophysical response of flood basalts from analysis of wire line logs: Ocean Drilling Program Site 642, Vøring volcanic margin. *Journal of Geophysical Research,* **99**, 9279–9296.

Planke, S. & Eldholm, O. 1994. Seismic response and construction of seaward dipping reflectors in flood basalts: Vøring volcanic margin. *Journal of Geophysical Research,* **99**, 9263–9278.

Purnell, G.W. 1992. Imaging beneath a high-velocity layer using converted waves. *Geophysics,* **57**, 1444–1452.

Richardson, K., White, R.S., England, R.W. & Fruehn, J. 1999. Crustal structure east of the Faroe Islands. *Petroleum Geoscience,* **5**, 161–172.

Roberts, A.W., White, R.S., Lunnon, Z.C., Christie, P.A.F., Spitzer, R. & iSIMM, Team 2005. Imaging magmatic rocks on the Faroes margin. *In:* Doré, A.G. & Vining, B. (eds) *Petroleum Geology: North-West Europe and Global Perspectives – Proceedings of the 6th Petroleum Geology Conference*. Geological Society, London, 755–766.

Schönberger, M. & Levin, F.K. 1974. Apparent attenuation due to intrabed multiples. *Geophysics,* **39**, 278–291.

Schönberger, M. & Levin, F.K. 1978. Apparent attenuation due to intrabed multiples, II. *Geophysics,* **43**, 730–737.

Spitzer, R., White, R.S. & Christie, P.A.F. 2003. Enhancing subbasalt reflections using parabolic t-p transformation. *The Leading Edge,* **22**, 1184–1201.

Sørensen, A.B. 2003. Cenozoic basin development and stratigraphy of the Faroes area. *Petroleum Geoscience,* **9**, 189–207.

Van der Baan, M., Kerrane, T., Kendall, J.M. & Taylor, N. 2003. Imaging sub-basalt structures using locally converted waves. *First Break,* **21**, 31–38.

White, N.J. & Lovell, B. 1997. Measuring the pulse of a plume with the sedimentary record. *Nature,* **387**, 57–71.

White, R. & McKenzie, D. 1989. Magmatism at rift zones: The generation of volcanic continental margins and flood basalts. *Journal of Geophysical Research,* **94**, 7685–7729.

White, R.S., Fruehn, J., Richardson, K.R., Cullen, E., Kirk, W., Smallwood, J.R. & Latkiewicz, C. 1999. Faeroes Large Aperture Research Experiment (FLARE): imaging trough basalt. *In:* Fleet, A.J. & Boldy, S.A.R. (eds) *Petroleum Geology of Northwest Europe: Proceedings of the 5th Conference*. Geological Society, London, 1243–1252.

White, R.S., Christie, P.A.F., Kusznir, N.J. *et al.* 2002. iSIMM pushes frontiers of marine seismic acquisition. *First Break,* **20**, 782–786.

White, R.S., Smallwood, J.R., Fliedner, M.M., Boslaugh, B., Maresh, J. & Fruehn, J. 2003. Imaging and regional distribution of basalt flows in the Faeroe–Shetland Basin. *Geophysical Prospecting,* **51**, 215–231.

White, R.S., Spitzer, R., Christie, P.A.F. & iSIMM, Group 2005. Seismic imaging through basalt flows on the Faroe Shelf. *In:* Ziska, H., Varming, T. & Bloch, D. (eds) Faroe Islands Exploration Conference: Proceedings of the 1st Conference. *Annales Societatis Scientiarum Færoensis,* Supplementum 43, Tórshavn, 11–31.

Ziolkowski, A. & Fokkema, J.T. 1986. Tutorial: The progressive attenuation of high-frequency energy in seismic reflection data. *Geophysical Prospecting,* **34**, 981–1001.

Ziolkowski, A., Parkes, G., Hatton, L. & Haugland, T. 1982. The signature of an air-gun array – Computation from near-field measurements including interactions. *Geophysics,* **47**, 1413–1421.

Ziolkowski, A., Hanssen, P., Gatliff, R. *et al.* 2003. Use of low frequencies for sub-basalt imaging. *Geophysical Prospecting,* **51**, 169–182.

Received 1 August 2004; revised typescript accepted 16 January 2005.